Vol. 00, No. 00, 00 Month 200x, 1–12

## RESEARCH ARTICLE

# Rescaled potentials for transition metal solutes in $\alpha$-iron

D.J. Hepburn[a]*, G.J. Ackland[a] and P. Olsson[b]

[a]School of Physics and Astronomy, University of Edinburgh, James Clerk Maxwell Building, King's Buildings, Mayfield Road, Edinburgh EH9 3JZ, United Kingdom;

[b]Département MMC, EDF-R&D, Les Renardières, F-77250 Moret sur Loing, France

()

We present empirical potentials for dilute transition metal solutes in $\alpha$-iron. They are in the Finnis-Sinclair form and are therefore suitable for billion atom molecular dynamics simulations. The potentials have been developed using a rescaling technique to provide solute-iron and solute-solute interactions from an existing iron potential. By fitting to first principles calculations, which show clear trends in the properties of transition metal solutes in iron across the series, we find trends in the rescaling parameters which, in principle, can be related to the elementary electronic properties of the solutes and in particular the occupancy of the *d*-electron band. We comment on the possibility of utilising such relationships to create multi-component potentials for transition metal solutes in $\alpha$-iron.

**Keywords:** Finnis-Sinclair ; empirical potential ; transition metal solute ; iron ; rescaling ; multi-component

## 1. Introduction

The ability to model many component alloys of iron on the atomic level would provide an extremely powerful tool for research into the behaviour of these materials. In particular it would allow the effects of varying proportions of solutes on the properties of these materials to be studied in detail. The theoretical insights gained would complement the already extensive understanding of such systems found from experiment and ultimately impact on the design of new materials to suit particular applications such as those for the nuclear industry.

In principle one would wish to model these materials using ab-initio electronic structure calculations but such techniques are prohibitive, being restricted to less that 1000 atoms and femto second timescales. Alternative higher level modelling

*Corresponding author. Email: dhepburn@ph.ed.ac.uk

ISSN: 1478-6435 print/ISSN 1478-6443 online

DOI: 10.1080/1478643YYxxxxxxxx
http://www.informaworld.com

techniques exist, such as kinetic monte-carlo (kMC) and molecular dynamics simulations (MD) using empirical potentials, that remove these restrictions but at the expense of requiring input from experiment or ab-initio calculations to fix their free parameters. In particular, empirical potentials allow billion atom simulations to be performed over nano second timescales. The results from such simulations are readily used as input to continuum engineering models and ultimately in the design of new materials.

The Finnis-Sinclair (FS) scheme [1] was based around the idea of a second moment model to the local density of states. In this model the band energy depends on the width of the band, the shape of the band, and the occupation of the band. The moments theorem [2] shows how band width can be determined from the sum of squares of hopping integrals, which forms the physical basis for the cohesive term in Finnis-Sinclair potentials. The band shape and occupation are implicitly assumed to be constant.

For elements in a single phase with charge neutrality [3], the $d$-band occupation is essentially constant, and the band shape does not change massively. This underlies the success of single-element potentials. Fitting to alloys has a more troubled history. Whereas isoelectronic alloys for isostructural elements work well [4], potentials for systems involving structural phase transitions or elements from different series tend to have poor transferability from the composition at which they are fitted. Potentials covering wide ranges of concentration are, however, possible [5] as are multi-component systems [6] although the inclusion of physics beyond the second moment approximation may be necessary in general. Difficulties also arise in the Finnis-Sinclair and related schemes such as the embedded atom method (EAM) [7–9] due to the increasing complexity of the model. For an $N$-component system the number of parametrised functions grows as $N^2$, as does the number of data points required to fit the parameters of these functions.

There is one important exception where the band shape and electron density are reasonably constant, and we might hope that the second-moment approach will work. That is multi-component alloys with one dominant element and multiple minority elements, a particularly relevant case here being steel. The dominant element fixes both the crystal structure and the electron density and should, in principle, connect the behaviour of single solute atoms to that of the dominant element and introduce stronger connections between solute-solute interactions and the properties of single solutes.

In this paper we present empirical potentials for single transition metal solutes in $\alpha$-iron by rescaling the functions of a pure iron potential. We also investigate ways to connect the interactions between solute particles to those of single solute atoms in iron which would allow multi-component potentials to be built once the interactions of single solutes in iron are known. We start by providing motivation for this procedure from the results of an ab-initio study and then give a detailed description of the rescaling strategy. We then discuss the results for single solute atoms in iron and present the findings of our investigation into solute-solute interactions. Finally we present our conclusions.

## 2. Rescaling

### 2.1. *Ab-initio calculations: Is rescaling credible?*

If the key physics of substitutional atoms in steel is such that a rescaling approach will work, we should expect that the rescaling will involve the $d$-electron density and the principal quantum number. Such an approach should work both for the perfect lattice and for defects. The properties of substitutional transition elements in Fe, in particular their magnetic character, have long been known to have systematic trends [11, 12]. Here we supplement this work with an emphasis on total energy calculations for substitutional atoms and their interactions with point defects in bcc Fe.

We use the VASP code [13] with projector augmented wave (PAW) pseudopotentials [14] and the generalised gradient approximation [15] with the Vosko-Wilk-Nusair interpolation [16], which we find to give the best compromise between computation speed and accuracy. This gives a lattice parameter for pure iron of 2.83Å, which was used in the impurity and defect calculations to define a fixed-volume supercell. Supercells of 128±1 atoms were used with a Monkhorst-Pack 3x3x3 k-point grid sampling the Brillouin zone. The energy cutoff was set to 300 eV. Full details of the calculations will be published elsewhere [10].

The following definition has been used for the binding energy of $n$ defects and impurities, $\{A_i\}$:

$$E_b(\{A_i\}) = \left[\sum_{i=1}^{n} E(A_i)\right] - \left[E(\{A_i\}) + (n-1)E_0\right], \tag{1}$$

where $E(A_i)$ is the energy for a configuration containing $A_i$ only, $E(\{A_i\})$ refers to a configuration containing all the interacting entities and $E_0$ refers to a configuration containing no defects or impurities i.e. bulk $\alpha$-iron.

The ab-initio total energy calculations show that there are systematic trends across the transition metal series for the free atom substitutional energy, $E_s$, excess pressure from a single solute, $P$, first nearest neighbour solute-iron separation, $r_{1\mathrm{nn}}$, solute-solute interactions, binding energies of a single solute to a vacancy defect at 1nn, $E_\mathrm{b}^{\mathrm{V,1nn}}$, and 2nn, $E_\mathrm{b}^{\mathrm{V,2nn}}$, separations and the binding energies to a $\langle 110\rangle$-self-interstitial defect in the mixed, $E_\mathrm{b}^{\mathrm{SI,M}}$, compressive, $E_\mathrm{b}^{\mathrm{SI,C}}$, and tensile sites $E_\mathrm{b}^{\mathrm{SI,T}}$, (see FIG. 1 for configurations) as shown in FIG. 2. The free atom substitutional energy was calculated from our ab-initio results for the substitution energy from the pure equilibrium phase and the experimental cohesive energies of the pure phases [17]. We take these values as fit targets in order to determine the parameters of our potentials, as discussed in the following section.

We plot all energies against the number of $d$-electrons in the free atom. In the solid this number will be affected by $s-d$ transfer of approximately 0.5 electrons per atom. Thus although there are clearly different trends with the 3d solutes for more-than or less-than half filled bands, rigorously defining which material corresponds to a half-filled $d$-band is not straightforward.

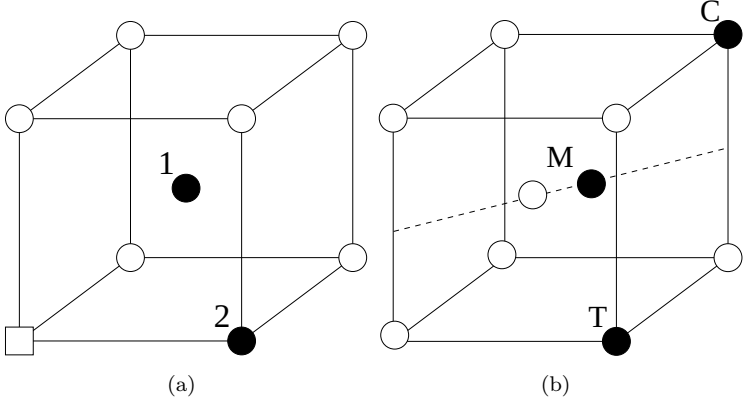


Figure 1. (a) First and second nearest neighbour solute sites (black) relative to a vacancy defect (square) (b) Mixed (M), compressive (C) and tensile (T) solute sites (black) relative to a ⟨110⟩-self-interstitial defect.

Two elements produce outlier behaviour: chromium and manganese. Curiously, iron chromium and manganese were elements which Finnis-Sinclair were unable to fit with their original scheme [1]. These elements exhibit unusual magnetic behaviour, which presumably accounts for this.

### 2.2. *Rescaling Strategy*

The starting point for our fitting strategy is the pure iron FS-type potential of Ackland *et al.* [18]. We have chosen this iron potential over those from more recent works [19–21] because it reproduces many of the properties of iron despite its relatively simple form.

The most general form for the energy, $U$, of an FS-type potential is given by

$$U(\{r_{ab}\}) = \sum_{a,b>a} V^{(X_a,X_b)}(r_{ab}) - \sum_a \sqrt{\rho_a}, \tag{2}$$

$$\rho_a = \sum_{b\neq a} \phi^{(X_a,X_b)}(r_{ab}), \tag{3}$$

where $V^{(X_a,X_b)}$, $\phi^{(X_a,X_b)}$ and $F^{(X_a)}$ are parametrised functions dependent on the atomic species, $X_a$ and $X_b$. The cross-species pair functions are taken to be symmetrical here, i.e. $V^{(X,Y)} \equiv V^{(Y,X)}$ when $X \neq Y$, as are the functions, $\phi^{(X,Y)}$.

We use the same forms for the component functions of our potential as used in the pure iron potential [18]. In particular we define the pair functions by

$$V^{(X,Y)}(r) = \begin{cases} \frac{Z_X Z_Y e^2}{4\pi\epsilon_0 r}\xi(r/r_s) & r \leq r_1 \\ \exp(B_0 + B_1 r + B_2 r^2 + B_3 r^3) & r_1 < r \leq r_2 \\ C^{(X,Y)}(r) = \sum_{k=1}^{6} a_k^{(X,Y)}(r_k^{(X,Y)} - r)^3 H(r_k^{(X,Y)} - r) & r > r_2 \end{cases} \tag{4}$$

where $Z_X$ is the atomic number of species $X$, $r_s = 0.88534\ a_b/\sqrt{Z_X^{2/3} + Z_Y^{2/3}}$, $a_b$ is

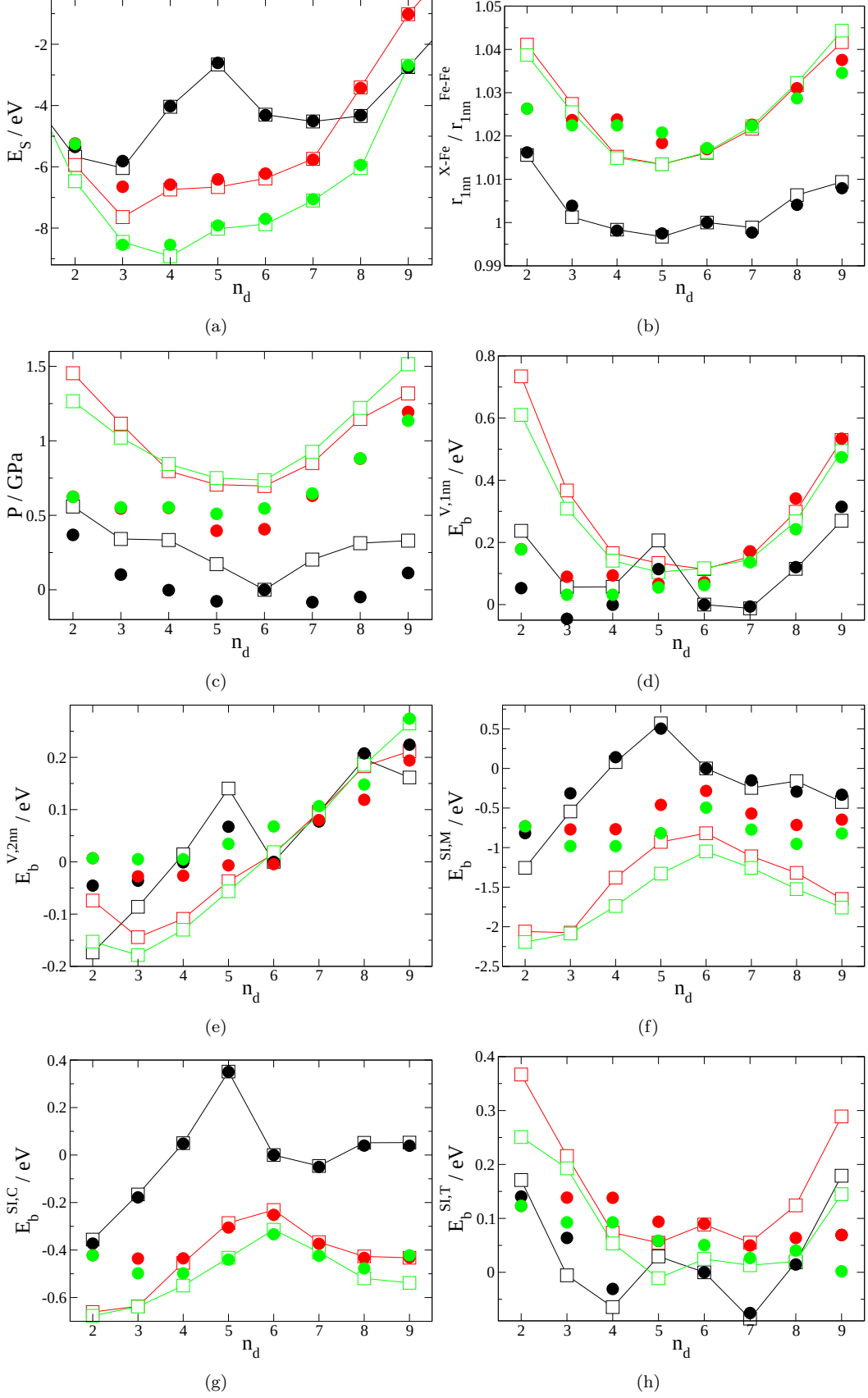


Figure 2. Fit targets (squares and lines), derived from our ab-initio data, and corresponding values from our empirical model (circles) versus number of d-electrons for 3d solutes (black), 4d solutes (red) and 5d solutes (green). The first nearest neighbour solute-iron separation, $r_{1\mathrm{nn}}^{X-\mathrm{Fe}}$, is plotted relative to the corresponding iron-iron separation, $r_{1\mathrm{nn}}^{\mathrm{Fe}-\mathrm{Fe}}$, in order to avoid thelattice parameter mismatch between ab-initio and the iron potential.

the Bohr radius and

$$\xi(x) = 0.1818e^{-3.2x} + 0.5099e^{-0.9423x} + 0.2802e^{-0.4029x} + 0.02817e^{-0.2016x}. \quad (5)$$

The functional form used below $r_1 = 0.9\mathring{\text{A}}$ is the universal screened potential of Biersack and Ziegler [22], above $r_2 = 1.9\mathring{\text{A}}$ is a parametrised cubic spline with cutoffs implemented by the use of Heaviside step functions, $H$, and between these is an interpolating function that ensures continuity of the function and its derivative.

The $\phi$ functions take the form of a simple cubic spline

$$\phi^{(X,Y)}(r) = \sum_{k=1}^{2} A_k^{(X,Y)}(R_k^{(X,Y)} - r)^3 H(R_k^{(X,Y)} - r). \quad (6)$$

For the pure iron component functions i.e. $V^{(\text{Fe,Fe})}$ and $\phi^{(\text{Fe,Fe})}$ we take the parameters directly from [18]. Iron-solute interactions are defined by rescaling these two functions using rescale parameters, $\{p_i^{(X)}\}$:

$$C^{(\text{Fe},X)}(p_1^{(X)} r) = p_2^{(X)} C^{(\text{Fe,Fe})}(r) \quad (7)$$

$$\phi^{(\text{Fe},X)}(p_3^{(X)} r) = p_4^{(X)} \phi^{(\text{Fe,Fe})}(r) \quad (8)$$

This is equivalent to a direct rescaling of the length and energy units of the cubic spline functions given by, for example,

$$r_k^{(\text{Fe},X)} = p_1^{(X)} r_k^{(\text{Fe,Fe})} \quad (9)$$

$$a_k^{(\text{Fe},X)} = \frac{p_2^{(X)}}{{p_1^{(X)}}^3} a_k^{(\text{Fe,Fe})}. \quad (10)$$

We take the rescaling factors, $\{p_i^{(X)}\}$, to be the adjustable parameters for the purposes of fitting. The trends in the fit target data should therefore translate to trends in these rescale parameters across the transition metal series. In fact it should be possible to quantify these trends by finding functional forms that relate the rescale parameters to the elementary electronic properties of the solutes. We present our results for these rescale parameters in the following section.

Solute-solute interactions can be defined by a similar rescaling procedure:

$$C^{(X,Y)}(p_1^{(X,Y)} r) = p_2^{(X,Y)} C^{(\text{Fe,Fe})}(r) \quad (11)$$

$$\phi^{(X,Y)}(p_3^{(X,Y)} r) = p_4^{(X,Y)} \phi^{(\text{Fe,Fe})}(r). \quad (12)$$

In principle it should be possible to relate these rescale parameters back to those for the solute-iron interactions and ultimately back to the electronic properties of the solutes. If such a relationship were found it would allow multi-component alloys to be immediately modelled. We present results for the rescale parameters,

$\{p_i^{(X,X)}\}$, and investigate the presence of any relationships between them and the iron-solute rescale parameters, $\{p_i^{(X)}\}$, in what follows.

## 3. Single solute interactions in iron

In order to determine the rescale parameters, $\{p_i^{(X)}\}$, we fit to the ab-initio data shown in FIG. 2 for transition metal solutes in $\alpha$-iron. We do not, however, fit to $E_{\mathrm{b}}^{\mathrm{SI,M}}$ as this is a strongly unfavoured position for most solutes and no satisfactory results were found with this quantity included.

The fitting procedure was accomplished by minimising a standard least squares response function, $\chi^2$, of the fit parameters, $\{p_i\}$, given in terms of the fit targets, $\{t_r\}$, model values, $\{m_r(\{p_i\})\}$, and weight factors, $\{\sigma_r\}$, by

$$\chi^2(\{p_i\}) = \sum_r \left( \frac{m_r(\{p_i\}) - t_r}{\sigma_r} \right)^2 . \tag{13}$$

Our potential model values were all calculated in atomically relaxed 4x4x4 bcc unit cell configurations, i.e. 128 atoms before the introduction of defects and solutes, at the equilibrium volume for the pure iron potential, i.e. $a_0 = 2.8665\mathring{\mathrm{A}}$ [18]. This was done in order to appropriately match the ab-initio fit target data. We chose weight factors of 0.01eV (or 1% of the fit target value if that was larger) for energies, $0.005\mathring{\mathrm{A}}$ for lengths and $5 \times 10^{-4}\mathrm{eV}/\mathring{\mathrm{A}}^3$ for pressures in our fits. The minimisation was accomplished using a local direct pattern search minimisation algorithm which is particularly useful when derivative information is time consuming to calculate, untrustworthy or non-existent. We have found this is a more trustworthy method when including particle separations for relaxed configurations in the fitting procedure. Initial parameter values for the direct search algorithm were found by evaluating the response function on a regularly spaced grid of points in parameter space and choosing the lowest one.

The fitted rescale parameters are given in FIG. 3 and TABLE. B1. It is immediately clear that there are trends across the series, especially for the 4d and 5d transition metal solutes. It has been necessary to use low order two-part piecewise polynomials to fit curves through the rescale parameters but it is difficult to say if this is due to some aspect of the underlying physics or just a result of the rescaling procedure. What is clear, however, is that the rescale parameters for manganese (3d,$n_d = 5$) show anomalous behaviour, consistent with the anomalous properties of the solute itself. Also clear is that the value of $p_4^{(\mathrm{Hf})}$ (5d,$n_d = 2$) is inconsistent with the trends shown. In some cases there are multiple minima of the response function, but this does not seem the case for hafnium. Attempts to modify $p_4^{(\mathrm{Hf})}$ to be consistent with the trend resulted in a very poor response function value and a further refit returned the rescale parameter to its previous value.

Looking at FIG. 2 we can see that the trends in the rescale parameters translate to the potential model values themselves. There is especially good reproduction of the substitution energy across all three series. The binding energy, $E_{\mathrm{b}}^{\mathrm{SI,C}}$, is reproduced almost as well but shows slight deviation from the ab-initio target data

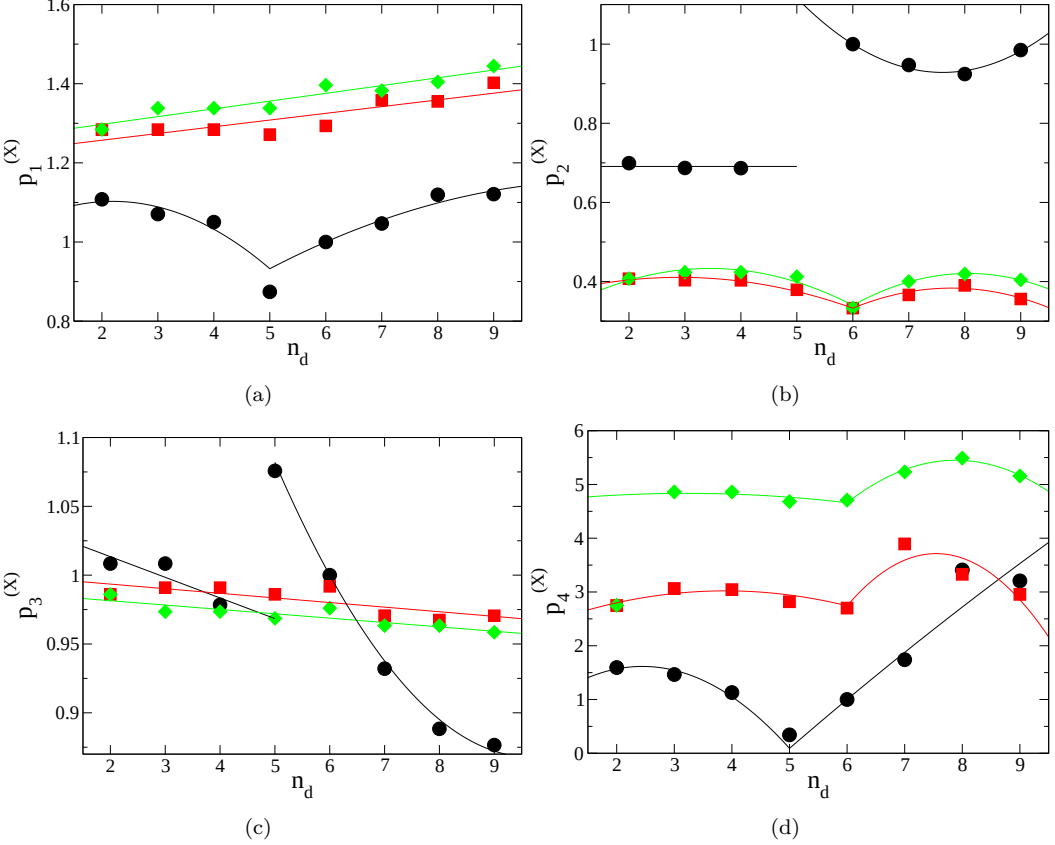


Figure 3. Rescale parameters as a function of the number of d-electrons for the 3d solutes (black circles and lines), 4d solutes (red squares and lines) and 5d solutes (green diamonds and lines). The graphs are for (a) $p_1^{(X)}$, (b) $p_2^{(X)}$, (c) $p_3^{(X)}$ and (d) $p_4^{(X)}$. The lines have been produced by fitting the rescale parameters to simple piecewise polynomial functions in order to guide the eye.

at the ends of the series and especially for low $n_d$. Such deviations from the usually parabolic trends in the ab-initio data are seen generally for the other fit targets. The most notable is for the binding energy, $E_{\mathrm{b}}^{\mathrm{SI,T}}$, where the potential models show approximately linear behaviour in $n_d$. The overall deviations and the quality of the fits is best quantified via the response function values, as shown in TABLE. B3. It is clear from this data that the potentials for the low $n_d$ solutes perform especially poorly. For these elements d-bonding is weakest: s-bonding is neglected in the Finnis-Sinclair concept but may play an important role here.

It is also clear from the response function data that the 3d solute potentials perform better overall than those of the other two series despite the presence of complex magnetic interactions. Even the anomalous properties of manganese are reproduced well. The excess solute pressures are, however, significantly underestimated although this is true of the 4d and 5d elements also.

Finally it is worth returning to the difficulties experienced in fitting the binding energy of the mixed interstitial, $E_{\mathrm{b}}^{\mathrm{SI,M}}$. As can be seen from FIG. 2(f) our potentials significantly underestimate the magnitude of this value for the 4d and 5d elements. Including this value in the fits did result in a more accurate reproduction but at too much cost to the reproduction of the other fit targets. Despite this the mixed site is still preserved as the least favoured for a solute to occupy around a $\langle 110 \rangle$-self-interstitial defect. This failure is unlikely to have serious consequences for any molecular dynamics simulations using our potentials, since the mixed dumbbell

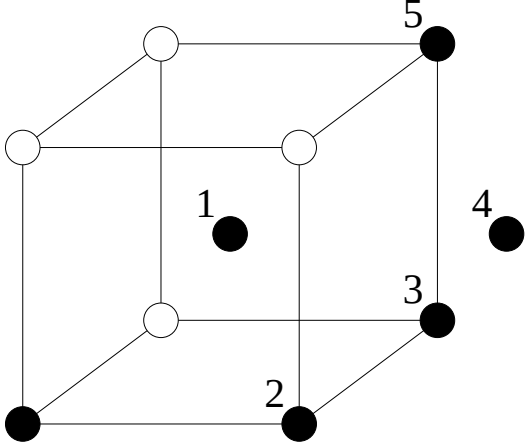


Figure 4. Solute positions (black) in bcc iron (white) for configurations with two interacting solute particles. The numbered solute particles show the first to fifth nearest neighbour positions relative to the unnumbered solute.

site is not a migration barrier. The interstitial is repelled by the solute by well above any realistic thermal energy and so the mixed interstitial site will occur with very low probability. Only for the 3d solutes is the binding energy low enough to significantly influence solute dynamics. In this case our potentials perform well, even reproducing the positive binding of chromium and manganese in the mixed interstitial, despite being excluded from the fit.

## 4. Solute-solute interactions in iron

In order to gain some insight into the possible relationship between the solute-solute rescale parameters and the solute-iron rescale parameters we have fitted the rescale parameters, $\{p_i^{(X,X)}\}$, to reproduce ab-initio values [10] for the solute-solute binding energies from 1nn to 5nn separation, $E_{\rm b}^{X-X,i{\rm nn}}$, and to the separations between solutes at 1nn separation, $r_{\rm 1nn}^{X-X}$, and 2nn separation, $r_{\rm 2nn}^{X-X}$ (see FIG. 4 for configurations). Our potential model values have been calculated in the same way as for the fits to the solute-iron rescale parameters and the same weight factors were used. The resulting values for the rescale parameters are shown in FIG. 5 and given in TABLE. B2, response function values are given in TABLE. B3 and our model values are compared with the ab-initio fit targets in FIG. 6.

The fit targets in FIG. 6 once again show a trend across the group and are well reproduced by our potentials. The picture emerging from the fit parameters themselves in FIG. 5 is less clear. For elements above half-filling there are clear trends with principal quantum number and $n_d$. However, for 5d elements with $n_d < 5$ there is considerable scatter for $p_2^{(X,X)}$ and $p_3^{(X,X)}$. It appears that a longer-ranged $\phi$ can compensate for a stronger repulsion. Since this anomaly is not present in the fit targets in FIG. 6, it must be an artifact of the fitting process itself and may well be due to the presence of multiple minima in the response function.

We have attempted to find any clear relationship between the solute-solute and solute-iron rescale parameters. However, even a direct plot of $p_i^{(X,X)}$ against $p_i^{(X)}$ showed no clear patterns. A functional dependence between the rescale parameters

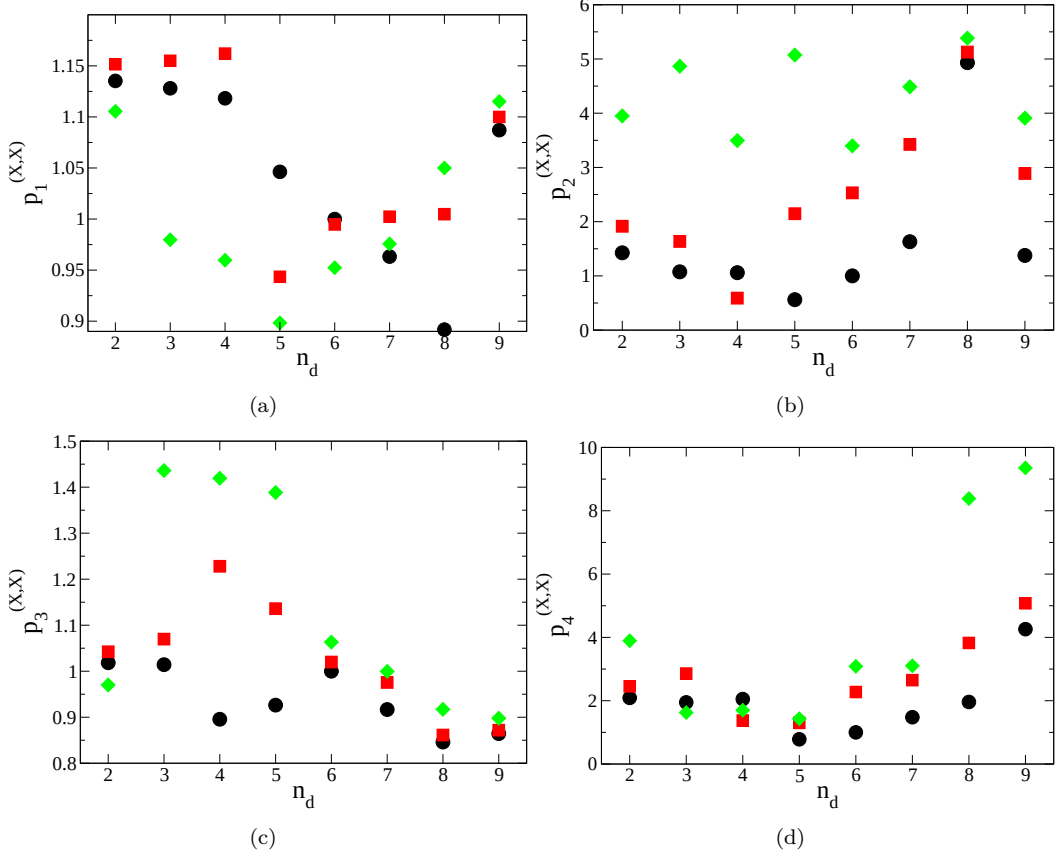


Figure 5. Rescale parameters as a function of the number of d-electrons for the 3d solutes (black circles), 4d solutes (red squares) and 5d solutes (green diamonds). The graphs are for (a) $p_1^{(X,X)}$, (b) $p_2^{(X,X)}$, (c) $p_3^{(X,X)}$ and (d) $p_4^{(X,X)}$.

was a necessary pre-requisite for the construction of a multi-component potential and we can conclude that this has not been possible in the current work. We have, however, produced binary potentials for transition metal solutes in $\alpha$-iron from a simple rescaling technique, many of which reproduce the ab-initio data to within the likely precision of such calculations.

## 5. Conclusions

In conclusion, we have advanced the hypothesis that the interactions between transition metal atoms in iron can be described by simply scaling the parameters of a Finnis-Sinclair model, and further that these scaling parameters are simply functions of the number of *d*-electrons and the principal quantum number. Quantum mechanical calculations of interactions between solutes and point defect show clear trends across the group. We have presented best-fit rescaled potentials for all transition metal elements in an iron matrix.

Our hypothesis is based on the notion that the environment around the impurity is close to that in magnetic bcc iron, hence we do not expect that the rescaled potentials will be transferable to very different electronic environments such as pure elements.

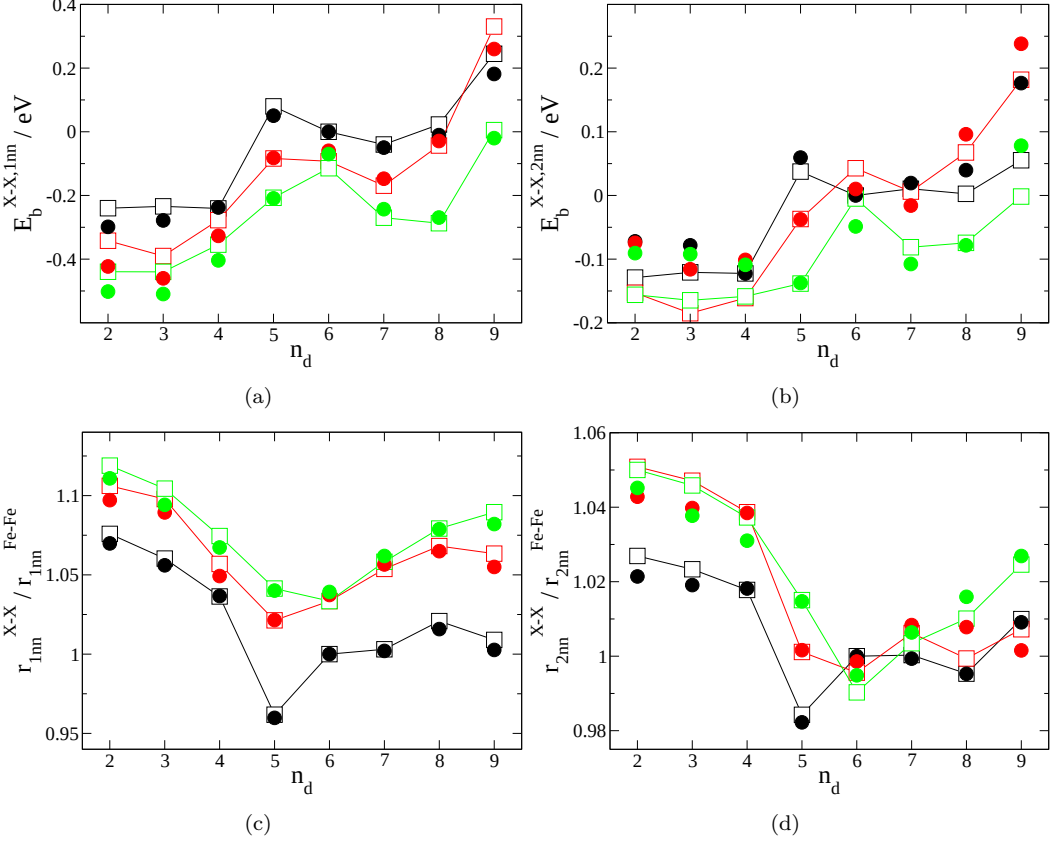


Figure 6. Solute-solute fit targets (squares and lines), derived from our ab-initio data, and corresponding values from our empirical model (circles) versus number of d-electrons for 3d solutes (black), 4d solutes (red) and 5d solutes (green).

## Acknowledgements

We gratefully acknowledge support from the EU FP7 GETMAT programme.

## References

[1] M.W. Finnis and J.E. Sinclair, Phil. Mag. A **50**, 45-55 (1984).
[2] Ducastelle and Cyrot-Lackmann Adv.Phys **16**, 393 (1967); J.Phys.Chem.Solids, 31, 1295 (1970)
[3] G. J. Ackland, M. W. Finnis, and V. Vitek, J. Phys. F **18**, L153 (1988).
[4] G. J. Ackland, G. I. Tichy, V. Vitek, and M. W. Finnis, Phil. Mag. A, **56**, 735 (1987).
[5] P. Olsson, J. Wallenius, C. Domain, K. Nordlund, L. Malerba, Phys. Rev. B **74**, 229906 (2006).
[6] Bonny *et al.*, submitted to Phil. Mag. Finnis-Sinclair special issue.
[7] M.S. Daw and M.I. Baskes, Phys. Rev. B **29**, 6443-6453 (1984).
[8] R.A. Johnson, Phys. Rev. B **39**, 12554-12559 (1989).
[9] G.J. Ackland and S.K. Reed, Phys. Rev. B **67**, 174108 (2003).
[10] P.Olsson, E.Vincent and C.Domain, in preparation
[11] V.I. Anisimov, V.P. Antropov, A.I. Liechtenstein, V.A. Gubanov and A.V. Postnikov, Phys. Rev. B **37**, 5598 (1988).
[12] B. Drittler, N. Stefanou, S. Blügel, R. Zeller and P.H. Dederichs, Phys. Rev. B **40**, 8203(1989).
[13] G. Kresse and J. Hafner, Phys. Rev. B **47**, 558 (1993); G. Kresse and J. Furthmuller, Phys. Rev. B **54**, 11 169 (1996).
[14] P.E. Blöchl, Phys. Rev. B **50**, 17953 (1994); G. Kresse and D. Joubert, Phys. Rev. B **59**, 1758 (1999).
[15] J.P. Perdew *et al.*, Phys. Rev. B **46**, 6671 (1992).
[16] S.H. Vosko, L. Wilk and M. Nusair, J. Can. Phys. **58**, 1200 (1980).
[17] J.D. Cox, D.D. Wagman and V.A. Medvedev, Codata Key Values for Thermodynamics, Hemisphere Pub. Corp., New York, (1989).
[18] G.J. Ackland, D.J. Bacon, A.F. Calder and T. Harry, Phil. Mag. A **75**, 713-732 (1997).
[19] M.I. Mendelev *et al.*, Phil. Mag. **83**, 3977-3994 (2003).

Table A1. Parameters for the pure iron potential [18].

| $k$ | $a_k^{\mathrm{Fe,Fe}}$ / eV$\mathring{\mathrm{A}}^{-3}$ | $r_k^{(\mathrm{Fe,Fe})}$ / $\mathring{\mathrm{A}}$ |
|---|---|---|
| 1 | -1.5522033 | 3.38247 |
| 2 | 2.649964948 | 3.296475 |
| 3 | -0.558542776 | 3.09582 |
| 4 | -0.115540092 | 2.837835 |
| 5 | 0.372003235 | 2.665845 |
| 6 | 4.245649731 | 2.482460633 |
| | $A_k^{\mathrm{Fe,Fe}}$ / eV$^2\mathring{\mathrm{A}}^{-3}$ | $R_k^{(\mathrm{Fe,Fe})}$ / $\mathring{\mathrm{A}}$ |
| 1 | 3.093735585 | 3.72645 |
| 2 | -4.285763266 | 3.4398 |


[20] G.J. Ackland, M.I. Mendelev, D.J. Srolovitz, S. Han and A.V. Barashev, J. Phys.:Condens. Matter **16**, S2629-S2642 (2004).
[21] M. Müller, P. Erhart and K. Albe, J.Phys.:Condens.Mater **19**, 326220 (2007).
[22] J.P. Biersack and J.F. Ziegler, Nucl. Instrum. Methods **194,** 93-100 (1982).


## Appendix A. Pure iron potential

The parameters for the pure iron potential of Ackland *et al.* [18] are given in TABLE. A1. It is worth pointing out that the function, $\phi(r)$, with these parameters actually has a maximum value at $r_{\max} = 1.82021002\mathring{\mathrm{A}}$ of $\phi(r_{\max}) = 3.222480407\mathrm{eV}^2$ and becomes negative for low separations. To avoid any possible problems this may cause the author recommends setting $\phi$ to its maximum value below $r_{\max}$. Such radii are only sampled under extreme conditions such as high pressures or in radiation damage simulations and this change will not modify any equilibrium or near equilibrium properties of the iron model.

## Appendix B. Rescale parameters and fit results

The fitted values for the rescale parameters for iron-solute, $p_i^{(X)}$, and solute-solute, $p_i^{(X,X)}$, interactions are given in TABLES. B1 and B2. The response function values for the respective fits are given in TABLE. B3.

Table B1. Rescale parameters for iron-solute interactions

| Solute, $X$ | $p_1^{(X)}$ | $p_2^{(X)}$ | $p_3^{(X)}$ | $p_4^{(X)}$ |
|---|---|---|---|---|
| Ti | 1.1079352022752937 | 0.69914888963867840 | 1.0084290227415416 | 1.5946911193111377 |
| V | 1.0704687944688829 | 0.68703519774868570 | 1.0084191748980367 | 1.4652839386546592 |
| Cr | 1.0504446925177677 | 0.68660606895558630 | 0.9784540205196225 | 1.1287695242404665 |
| Mn | 0.8740657069080267 | 2.37899559818691970 | 1.0757805626557944 | 0.3418424453237209 |
| Co | 1.0467024050842750 | 0.94717978096230060 | 0.9320535734737820 | 1.7396896806120596 |
| Ni | 1.1194809316877880 | 0.92438826748289380 | 0.8883635622171985 | 3.4100636005122293 |
| Cu | 1.1208802828524023 | 0.98505124753645820 | 0.8765649836565008 | 3.2065254293566600 |
| Zr | 1.2841655075134310 | 0.40739377742609160 | 0.9860071367651349 | 2.7482154017401133 |
| Nb | 1.2841655075134310 | 0.40336016805208613 | 0.9909619464976229 | 3.0647879434909940 |
| Mo | 1.2841655075134310 | 0.40306261907883430 | 0.9909619275965241 | 3.0437240549628903 |
| Tc | 1.2714509975380506 | 0.37927270590314116 | 0.9860317313257698 | 2.8186046924493455 |
| Ru | 1.2932752539714167 | 0.33285431259332965 | 0.9918471983137220 | 2.7002031043018238 |
| Rh | 1.3583482886258411 | 0.36634462066369505 | 0.9706236772142814 | 3.8933887256877090 |
| Pd | 1.3551721040070680 | 0.39024726568702440 | 0.9674492344138608 | 3.3285717131180084 |
| Ag | 1.4023136316534160 | 0.35592505640677500 | 0.9705185530509607 | 2.9551289346288447 |
| Hf | 1.2841655075134310 | 0.40746747208599430 | 0.9860071367651349 | 2.7521572914348287 |
| Ta | 1.3381889417068988 | 0.42350948842405384 | 0.9734862986585047 | 4.8610714605878340 |
| W | 1.3381889417068988 | 0.42350948842405384 | 0.9734862986585047 | 4.8610567185373155 |
| Re | 1.3381889417068988 | 0.41247111384741486 | 0.9686430832422932 | 4.6812582679644960 |
| Os | 1.3963331257722620 | 0.33347841442944126 | 0.9760396335905974 | 4.7084791631263130 |
| Ir | 1.3825438675169937 | 0.40034598076904200 | 0.9633439996351745 | 5.2329577841196330 |
| Pt | 1.4045418753797260 | 0.41926814851469420 | 0.9633439996351745 | 5.4900896361876255 |
| Au | 1.4447702630891220 | 0.40420070742435266 | 0.9585272796369986 | 5.1583042920958950 |

Table B2. Rescale parameters for solute-solute interactions

| Solute,$X$ | $p_1^{(X,X)}$ | $p_2^{(X,X)}$ | $p_3^{(X,X)}$ | $p_4^{(X,X)}$ |
|---|---|---|---|---|
| Ti | 1.135234375 | 1.425375 | 1.0184375 | 2.090625 |
| V | 1.128015625 | 1.07515625 | 1.01421875 | 1.9471875 |
| Cr | 1.1182627956431268 | 1.0591971435622631 | 0.8956061196601681 | 2.0520677210215306 |
| Mn | 1.04625 | 0.561 | 0.926296875 | 0.78140625 |
| Co | 0.9632660156249979 | 1.63034375 | 0.916725 | 1.47909375 |
| Ni | 0.8917071437428479 | 4.931618183795954 | 0.846 | 1.9593257026672335 |
| Cu | 1.087078125 | 1.3775 | 0.864421875 | 4.26 |
| Zr | 1.1515625 | 1.915 | 1.04225 | 2.455375 |
| Nb | 1.155 | 1.63625 | 1.06975 | 2.859375 |
| Mo | 1.16200390625 | 0.590203125 | 1.228046875 | 1.374328125 |
| Tc | 0.94346875 | 2.1465625 | 1.135921875 | 1.299375 |
| Ru | 0.9946875 | 2.5315625 | 1.0199765625 | 2.275625 |
| Rh | 1.00234375 | 3.425 | 0.9755625 | 2.648625 |
| Pd | 1.00478125 | 5.126925 | 0.8613123046875 | 3.8247 |
| Ag | 1.1 | 2.889 | 0.871875 | 5.07775 |
| Hf | 1.1055 | 3.95 | 0.9700625 | 3.894 |
| Ta | 0.97971796875 | 4.86585 | 1.436123959960937 | 1.625 |
| W | 0.9597262573242189 | 3.4952026367187496 | 1.4194162597656252 | 1.6996997070312496 |
| Re | 0.8983463569335935 | 5.072334990624995 | 1.388288172737312 | 1.431971765625 |
| Os | 0.952375 | 3.3975 | 1.0632097695312475 | 3.085089 |
| Ir | 0.9756723193359381 | 4.48695 | 0.9996396093750014 | 3.10280625 |
| Pt | 1.05 | 5.385 | 0.917125 | 8.385 |
| Au | 1.115125 | 3.90925 | 0.89775 | 9.355 |

Table B3. Response function values, $\chi^2$, for the solute-iron rescale parameters given in TABLE. B1 and the solute-solute rescale parameters given in TABLE. B2.

| Solute,$X$ | $\chi^2(X-\mathrm{Fe})$ | $\chi^2(X-X)$ |
|---|---|---|
| Ti | 568.967 | 96.770 |
| V | 221.205 | 58.907 |
| Cr | 99.636 | 33.934 |
| Mn | 178.812 | 17.056 |
| Co | 43.902 | 2.755 |
| Ni | 65.728 | 32.237 |
| Cu | 204.809 | 204.468 |
| Zr | 4796.904 | 284.391 |
| Nb | 1689.753 | 208.931 |
| Mo | 216.139 | 88.197 |
| Tc | 137.204 | 9.579 |
| Ru | 69.618 | 36.145 |
| Rh | 26.411 | 104.771 |
| Pd | 103.652 | 61.308 |
| Ag | 477.687 | 142.646 |
| Hf | 3491.843 | 182.800 |
| Ta | 1502.974 | 152.638 |
| W | 408.336 | 76.466 |
| Re | 198.776 | 1.503 |
| Os | 85.532 | 261.420 |
| Ir | 35.811 | 284.450 |
| Pt | 69.882 | 302.596 |
| Au | 386.018 | 186.895 |